Controllability Properties of Solar Sails

Alesia Herasimenka, Lamberto Dell'Elce, Jean-Baptiste Caillau, Jean-Baptiste Pomet

Controllability Properties of Solar Sails

Alesia Herasimenka[1], Lamberto Dell'Elce[2], Jean-Baptiste Caillau[3], and Jean-Baptiste Pomet[4]

Trajectory design and station keeping of solar sails about a celestial body can be formulated as control problems with positivity constraints. Specifically, when re-emitted radiation is neglected and the sail is modeled as a flat surface, which are reasonable assumptions for control purposes, force generated by solar radiation pressure is contained in a pointed convex cone of revolution with axis towards the Sun-satellite direction. Therefore, classical approaches to infer controllability based on the Lie algebra rank condition do not apply to these problems. This study offers a novel condition to decide on controllability of control systems with positivity constraints. This condition is effective as it can be verified by solving an auxiliary convex optimization problem for which reliable numerical methods are available. A crucial ingredient of this approach is the theory of positive trigonometric polynomials. The practical interest of this condition is the assessment of a minimum requirement on the optical properties of the sail, which may be of use for mission design purposes.

[1] PhD student, Université Côte d'Azur, CNRS, Inria, LJAD; alesia.herasimenka@univ-cotedazur.fr.
[2] Researcher, Université Côte d'Azur, Inria, CNRS, LJAD
[3] Professor, Université Côte d'Azur, CNRS, Inria, LJAD
[4] Senior researcher, Université Côte d'Azur, Inria, CNRS, LJAD

I. Introduction

Solar sails offer a propellant-less solution to achieve interplanetary transfers, planet escapes, and de-orbiting maneuvers by leveraging on solar radiation pressure (SRP) [1]. Although very few solar sail missions were launched, the possibility to use SRP as an inexhaustible source of propulsion attracted the interest of researchers since decades, and several contributions on the guidance and control of solar sails are available. Specifically, a large body of literature focuses on the mathematical formulation and numerical solution of optimal interplanetary transfers (mostly minimum time) using optimization techniques [2], indirect methods [3] or even neural networks [4]. In addition, several contributions investigate locally optimal maneuvers, *i.e.*, maximization of the instantaneous rate of change of a desired orbital element, in particular increasing semi-major axis for orbit-raising [5] or decreasing perigee altitude for de-orbiting applications [6]. Classical feedback algorithms are also used to find sub-optimal trajectories, as for instance Q-law in [7]. Direct methods are often preferred to tackle the numerical solution of optimal control problems (OCP) of solar sail transfers [8] because they do not require an initial guess of adjoint variables, differently of indirect techniques, which were used in very few studies like [9] and [10].

Surprisingly enough, very few studies on the controllability of solar sails are available to date, although an analysis of the reachable set of passive sails was discussed in [11]. Most often, solutions of two-point boundary value problems coming for instance from optimal control are investigating without assessing beforehand whether the targeted point is within the reachable set of the control system from the initial point; exhibiting a solution of the two-point boundary value problem obviously proves reachability as a side result, but it is better to be able to certify non controllability and seek for solutions only when controllability holds.

A major difficulty in assessing the controllability of an SRP-actuated system is that the sail

cannot generate a force with a positive component toward the direction of the Sun, so that classical tools of geometric control theory cannot be used. For example, Lie algebra of the system is full rank (unless a fully absorptive model of the sail is considered), but although it should indicate that the system is weakly controllable, theory requires that the control set is a neighborhood of the origin, *i.e.*, both positive and negative controls should be generated, so that it is not sufficient to analyze the sailing problem. This aspect is particularly critical when considering a non-ideal sail (by ideal, we mean a perfectly reflective flat surface) because the control set is contained inside a strictly convex cone of revolution, whose angle depends on the optical properties of the sail.

The main contribution of the paper consists in a controllability check for non-ideal solar sails in a planet-centered orbit. This requirement is aimed at assessing whether the sail at hand is capable of decreasing or increasing all possible functions of the Keplerian integrals of motion over an orbital period. Given some optical properties, a convex cone containing all possible directions of the SRP is first defined. Then, the condition is verified by means of a worst-case optimization problem characterized by a finite number of design variables and a two-parameter family of inequality constraints, namely, the clock angle of the convex cone and the true anomaly of the sail. Numerical solution of this semi-infinite problem is achieved by leveraging on the formalism of squared functional systems [12, 13] to exactly enforce inequality constraints for all values of the true anomaly and the clock angle. No discretization is done to solve the problem numerically. Eventually, the semi-infinite problem is recast into a finite-dimensional convex programming with a finite number of linear matrix inequalities (LMI) and an unique well-defined solution. Non-satisfaction of the condition entails some local non-controllability of the system for the given value of the cone angle (and, consequently, of the optical properties) and orbital conditions. Hence, a fine analysis covering (as much as possible numerically) the entire phase space of orbital elements is carried out to determine

the minimum cone angle for a large range of orbits. It is shown that a universal (namely, planet independent) minimum angle exists that satisfies the condition for all orbits. Its value is about 60 degrees (note that 0 and 90 degrees correspond to fully absorptive and perfectly reflective sails, respectively). The result indicates that the sail does not have to be ideal to satisfy the requirement. The methodology is unaware of the specific source of non-ideality of the sail (e.g., specular or diffuse reflection, re-emitted radiation [1]) since it only uses the conical hull of the control set. This result can be used to provide insight into the controllability of the sail during its lifetime, owing to the degradation of its optical properties discussed in [14], and may support the design of real-life missions by serving as a minimal requirement to be satisfied.

Section II introduces the dynamical model of solar sails, geometry of the problem, equations of motion, and various assumptions used in this work. Section III outlines the novel condition for investigating local controllability of systems with peculiar constraints on the control set that apply to solar sails. An efficient numerical methodology based on convex programming to evaluate the aforementioned condition is detailed in section IV. Finally, this methodology is extensively used in Section V to deduce minimal requirements on the optical properties of solar sails. Controllability of heliocentric orbits is briefly discussed as well.

II. Dynamics of a solar sail

A. Force model

Solar sails use SRP as propulsive means to control their trajectory. SRP is due to the interaction between photons and surface of the sail. The magnitude of the pressure depends on the Sun-sail distance, $r_\odot$ (in AU). Specifically, denoting by $\Phi_{SR} \approx 1367$ W m^{-2} the solar flux at $r_\oplus = 1$ AU

and by c the speed of light, a simple model is [15, Chap. 3]:

$$P_{SR} = \frac{\Phi_{SR}}{c} \left(\frac{r_\oplus}{r_\odot}\right)^2$$

A flat sail with surface A and mass m is considered in this work. The resulting force depends on various optical and geometrical properties of the sail and it is obtained by summing up contributions of the incoming, reflected, and thermal radiations, namely $\boldsymbol{f}_a$, $\boldsymbol{f}_r$, and $\boldsymbol{f}_e$. In addition, the reflected force is divided into specular and diffuse components, $\boldsymbol{f}_{rs}$ and $\boldsymbol{f}_{ru}$, respectively. The first one is caused by photons that are reflected symmetrically with respect to the normal of the sail and create moment in the opposite direction. Conversely, diffuse reflection stems from surface roughness, which causes photons to be uniformly reflected in all directions, yielding a component of the force toward the vector normal to the sail. Finally, absorbed photons are then re-radiated in all directions with energy dependent on the temperature of the sail, generating another component of the force that is orthogonal to its surface. Figure 1a shows the directions of the various components. Denoting by $\hat{\boldsymbol{s}}$ the direction of the Sun, $\hat{\boldsymbol{n}}$ the unit vector normal to the sail with positive projection toward $\hat{\boldsymbol{s}}$, *i.e.*, $\cos\beta := \hat{\boldsymbol{n}} \cdot \hat{\boldsymbol{s}} \geq 0$, and

$$\hat{\boldsymbol{t}} := \frac{\hat{\boldsymbol{n}} \times \hat{\boldsymbol{s}}}{\|\hat{\boldsymbol{n}} \times \hat{\boldsymbol{s}}\|} \times \hat{\boldsymbol{n}} = \frac{\hat{\boldsymbol{s}} - \cos\beta\, \hat{\boldsymbol{n}}}{\sin\beta}$$

the tangent unit vector in the plane generated by $\hat{\boldsymbol{s}}$ and $\hat{\boldsymbol{n}}$, the components of the specific force are [16]

$$\begin{aligned}
\boldsymbol{f}_a &= \varepsilon(r_\odot)\, \cos\beta(\cos\beta\, \hat{\boldsymbol{n}} + \sin\beta\, \hat{\boldsymbol{t}}) \\
\boldsymbol{f}_{rs} &= \varepsilon(r_\odot)\, \rho\, s\, \cos\beta(\cos\beta\, \hat{\boldsymbol{n}} - \sin\beta\, \hat{\boldsymbol{t}}) \\
\boldsymbol{f}_{ru} &= \varepsilon(r_\odot)\, B_f\, \rho(1-s) \cos\beta\, \hat{\boldsymbol{n}} \\
\boldsymbol{f}_e &= \varepsilon(r_\odot)\, (1-\rho) \frac{\varepsilon_f B_f - \varepsilon_b B_b}{\varepsilon_b + \varepsilon_f} \cos\beta\, \hat{\boldsymbol{n}}
\end{aligned} \tag{1}$$

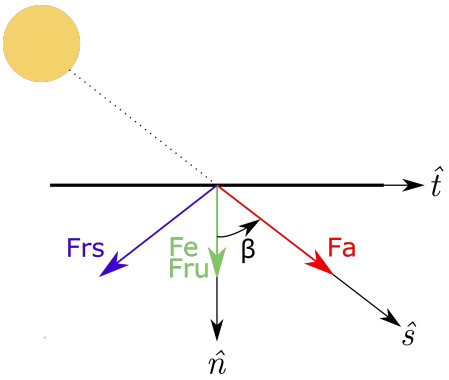

(a) Schematic representation.

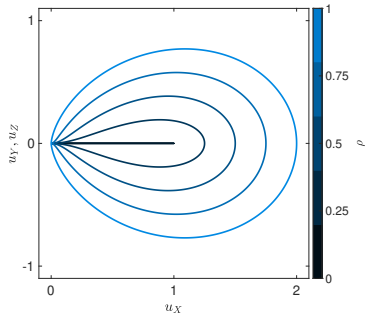

(b) Control sets for different reflectivity coefficients and $s = 1$. Here, u_X is the projection of $\boldsymbol{u}$ towards $\hat{\boldsymbol{s}}$, while u_Y and u_Z are orthogonal components.

Fig. 1: Components of the SRP force.

where the function $\varepsilon(r_\odot) = AP_{SR}m^{-1}$ has small magnitude, $\rho \in [0, 1]$ is the portion of reflected radiation, $s \in [0, 1]$ the fraction of specular reflection, and ε_b, ε_f, B_b, B_f are back and front surface emissivity and Lambertian coefficients, respectively. The resulting force is thus

$$\boldsymbol{f}_{SRP} = \boldsymbol{f}_a + \boldsymbol{f}_{rs} + \boldsymbol{f}_{ru} + \boldsymbol{f}_e.$$

B. Parametrization of the control set

Controlling the sail attitude, *i.e.* the normal vector $\hat{\boldsymbol{n}}$, allows to change the direction and magnitude of the resulting SRP. A reliable inference of optical coefficients is indeed mandatory to accurately estimate the mapping between $\hat{\boldsymbol{n}}$ and $\boldsymbol{f}_{SRP}$.

To carry out controllability analysis, solar sail dynamics is conveniently modeled as a nonlinear control-affine system (see Section II C), where the control variable is homogeneous to the force

vector, namely $\boldsymbol{u} := \dfrac{\boldsymbol{f}_{SRP}}{\varepsilon(r_\odot)}$. Control set $U \subset \mathbb{R}^3$ is then given by:

$$U = \left\{ \frac{\boldsymbol{f}_{SRP}(\hat{\boldsymbol{n}})}{\varepsilon(r_\odot)},\ \hat{\boldsymbol{n}} \in \mathbb{R}^3,\ \|\hat{\boldsymbol{n}}\| = 1 \right\}.$$

Figure 1b shows the projection of U on the plane generated by $\hat{\boldsymbol{n}}$ and $\hat{\boldsymbol{s}}$ for various optical properties. The set is a surface of revolution with axis $\hat{\boldsymbol{s}}$, and it is non-convex unless $\rho = s = 1$. Note that the interior of the surface is not part of U. When re-emitted radiation is neglected, which is most often a reasonable assumption for control purposes, U contains the origin but mapping between $\hat{\boldsymbol{n}}$ and $\boldsymbol{u}$ is non-smooth at this point. Two extreme cases can be identified: ideal sails are constituted by perfectly reflective surfaces ($\rho = s = 1$), whereas perfectly-absorptive surfaces are the worst-case scenario ($\rho = 0$, $\boldsymbol{f}_e$ neglected) because SRP is systematically parallel to $\hat{\boldsymbol{s}}$. Although sails are designed to be as ideal as possible, partial absorption of the energy is unavoidable in real-life applications and, in addition, optical properties exhibit degradation with time. Hence, the fraction of reflected radiation decreases with lifetime of the satellite, as discussed in [14].

C. Equations of motion

Controllability of a solar sail in orbit around a celestial body is considered in this study. The following assumptions are introduced:

1. Orbital period of the sail is much smaller than the one of the heliocentric orbit of the attractor, so that variations of the Sun direction $\hat{\boldsymbol{s}}$ over a single orbit of the sail are neglected.

2. Solar eclipses are neglected. Targeting a certification of non-controllability in Section III, this assumption is conservative, and it has the major advantage of yielding results that are independent of the semi-major axis of the orbit.

3. Re-emitted radiation is neglected. In fact, this component of SRP can be reasonably regarded

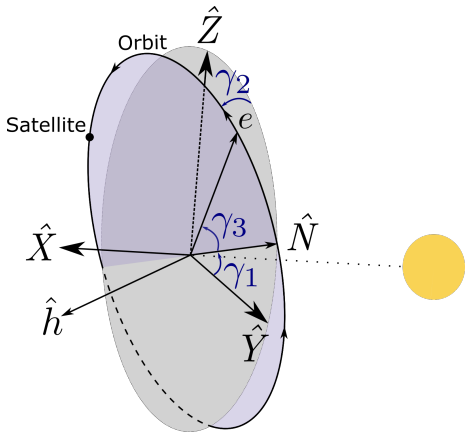

Fig. 2: Euler angles orienting the orbit with respect to the reference frame. Here, $\boldsymbol{h}$ and $\boldsymbol{e}$ denote the angular momentum and eccentricity vectors.

as a disturbance for control purposes.

Equations of motion are written in a set of Keplerian-like orbital elements, which leverages on the axial symmetry of the problem with respect to the Sun's direction. Namely, consider a reference frame with origin at the center of the planet, $\hat{\boldsymbol{X}}$ axis towards $\hat{\boldsymbol{s}}$, whereas $\hat{\boldsymbol{Y}}$ and $\hat{\boldsymbol{Z}}$ are arbitrarily chosen and form a right-hand frame. Because this study focuses on short-time controllability (time is of the order of one orbital period), motion of this frame is neglected by virtue of the first assumption above. Let γ_1, γ_2, γ_3 be Euler angles orienting the eccentricity vector according to a $X-Y-X$ rotation as depicted in Fig. 2, and a, e, and f be semi-major axis, eccentricity and true anomaly, respectively. Motion of slow elements, $I = (\gamma_1, \gamma_2, \gamma_3, a, e)^T \in M$, is governed by

$$\begin{aligned} \frac{\mathrm{d}\, I}{\mathrm{d}\, t} &= \varepsilon(r_\odot)\sqrt{\frac{a\left(1-e^2\right)}{\mu}} G(I,f)\, R(I,f)\, \boldsymbol{u} \\ \frac{\mathrm{d}\, f}{\mathrm{d}\, t} &= \omega(I,f) + \varepsilon(r_\odot) F(I,f)\, R(I,f)\, \boldsymbol{u} \end{aligned} \tag{2}$$

where components of $\boldsymbol{u}$ are in the reference frame, $R(I,f) = R_X(\gamma_3 + f)R_Y(\gamma_2)R_X(\gamma_1)$ is the

rotation matrix from reference to local-vertical local-horizontal frames[5], $\omega(I,f)=\sqrt{\frac{\mu}{a\,(1-e^2)^3}}(1+e\cos f)^2$, both $F(I,f)$ and $G(I,f)$ can be deduced from Gauss variational equations (GVE) of classical elements, where $G(I,f)$ is:

$$G=\begin{pmatrix} 0 & 0 & \dfrac{\sin(\gamma_3+f)}{\sin\gamma_2(1+e\cos f)} \\ 0 & 0 & \dfrac{\cos(\gamma_3+f)}{1+e\cos f} \\ -\dfrac{\cos f}{7}te & \dfrac{2+e\cos f}{1+e\cos f}\dfrac{\sin f}{e} & \dfrac{\cos(\gamma_3+f)}{1+e\cos f} \\ \dfrac{2\,a\,e}{1-e^2}\sin f & \dfrac{2\,a\,e}{1-e^2}(1+e\cos f) & 0 \\ \sin f & \dfrac{e\cos^2 f+2\cos f+e}{1+e\cos f} & 0 \end{pmatrix}$$

The peculiar choice of Euler angles follows from the symmetry of System (2), and it has the main consequence that controllability results in Section V are independent of γ_1. We also note that $(1+e\cos f)\,G(I,f)R(I,f)$ is a trigonometric polynomial in f. This has significant advantages for the numerical methodology detailed in Section IV.

Finally, orbital perturbations (other than SRP) are not included in Eq. (2) because we are interest in investigating geometric obstructions to the controllability of solar sails regardless their size.

III. Controllability of a solar sail

We are interested in studying obstructions to controllability of solar sails in orbit about a celestial body. More precisely, we want to assess the existence of variations of the current orbital elements set that a sail cannot generate after a single orbital period.

The classical approach to inspect controllability of control-affine systems with periodic drift

[5] Here, $R_A(\varphi)$ denotes the rotation matrix of angle φ about the axis $\hat{\boldsymbol{A}}$.

is detailed in [17] and [18, Chap. 4]. Specifically, global controllability (that is existence of an admissible control steering the system from any initial point towards any target) is guaranteed (sufficient condition) provided:

1. the drift of the system is periodic (or, more generally, recurrent);
2. the Lie algebra rank condition (LARC) condition holds, namely the set of vector fields defining the control-affine system are bracket generating;
3. the convex hull of the control set U is a neighborhood of the origin in $\mathbb{R}^m$.

Keplerian motion satisfies the first condition. Two different cases are distinguished for the computation of the rank of Lie algebra: First, *perfectly-absorptive sails* (*i.e.*, $\rho = 0$) are such that the control set degenerates to a segment aligned to $\hat{\boldsymbol{s}}$, as shown in Fig. 1b. Appendix A offers a detailed evaluation of Lie brackets in this case, which shows that the algebra is rank deficient. This allows to conclude the non-controllability of the system and to deduce an integral of motion, namely the projection of the angular momentum towards $\hat{\boldsymbol{s}}$ [19, Chap. 12]. Second, *real-life sails* are such that ρ is strictly positive and smaller than 1. In this case, control set is no more degenerate and the system is bracket generating. Nevertheless, controllability of this system cannot be assessed because U does not contain the origin in its interior (the origin is on the boundary of the control set as depicted in Fig. 1b), so that the third condition above is not satisfied, and the classical approach cannot be used to investigate controllability of this system.

A novel sufficient condition relaxing the third requirement was proposed in [20] and [21]. System (2) is controllable wrt. to the slow variables, meaning that there exists an admissible control allowing to reach any final orbit from any initial one,[6] if the control set U contains the origin (even

[6] Clearly, because of the periodicity of the free motion, the angular position determined by the true anomaly does

only on its boundary), and if for all I in M the following condition holds:

$$\operatorname{cone}\left\{\frac{\mathrm{d}\, I(f,I,\boldsymbol{u})}{\mathrm{d}\, t},\ \boldsymbol{u}\in U,\ f\in\mathbb{S}^1\right\}=T_I M. \tag{3}$$

Here before the operator cone indicates the conical hull: for a subset A of a vector space, cone(A) is the set of linear combinations with nonnegative coefficients of vectors of A,

$$\sum_{i=1}^{k}\lambda_i x_i,\quad k\in\mathbb{N},\quad \lambda_1,\dots,\lambda_k\geq 0.$$

It is always a convex pointed (containing the origin) cone. This result is proved in [20, 21]. If (3) only holds at one point, it remains true around it and controllability in the corresponding neighborhood follows. Conservely, (3) cannot hold if, for some orbit I_0, there exists a nonzero one-form $p_{I0}\in T^*_{I_0}M$ such that

$$\left\langle p_{I0},\ \frac{\mathrm{d}\, I(f,I_0,\boldsymbol{u})}{\mathrm{d}\, t}\right\rangle>0,\qquad f\in\mathbb{S}^1,\ \boldsymbol{u}\in U. \tag{4}$$

In this case, there is an obstruction to local controllability in the following sense: one can find a neighborhood of I_0 on which motion is prescribed to a half-space (see Fig. 3); orbits in the forbidden neighborhood half might be reached (*e.g.* if global controllability holds), but only by trajectories that must leave this neighborhood. For a detailed discussion on the gap between (3) and (4), we refer to [21].

IV. Numerical methodology to inspect local controllability

Given some optical properties of the sail and orbital state I, we are interested in determining if Eq. (4) has any non-trivial solution $p_I\neq 0$. Two manipulations are introduced to facilitate this task.

not play any role; any initial/final longitude can be departed from/reached, up to some additional time spent along the periodic initial/final orbit.

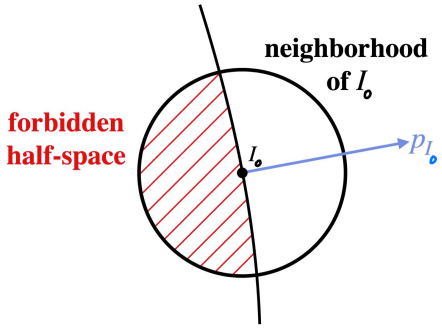

Fig. 3: Schematic representation of a half-space of the neighborhood of I where motion is (locally) forbidden.

First, the time derivative of I in Eq. (4) is replaced by $\tilde{G}(I,f)\boldsymbol{u}$, where

$$\tilde{G}(I,f) := (1 + e\cos f)G(I,f)R(I,f),$$

which is a second-degree trigonometric polynomial in f. Such property offers major benefits when positivity constraints are numerically enforced in Section IV B. This operation has no impact on the sign of Eq. (4). We also note that System (2) is axially symmetric with respect to the Sun-planet direction, and that semi-major axis and planetary constant have no impact on the sign of Eq. (4). Hence, *all outcomes of this controllability study are independent of both the semi-major axis and* γ_1 *(because of symmetry), and they are valid for any attractor (spherical symmetric central body), since magnitude of SRP does not impact the non-controllability condition (which is a geometric obstruction).*

Second, control set U is replaced by its conical hull, $K_\alpha := \text{cone}(U)$, which is a cone of revolution of angle α, as illustrated in Fig. 4. This approximation makes the problem convex (in fact, convex programming is used to get numerical certifies of the feasibility problem in Section IV A). Replacing

U by K_α has no impact on the closure of the reachable set of the control system, as discussed in [21]. Therefore, non-controllability of the system with controls in K_α implies non-controllability of the system with the original control set, U. Neglecting thermal radiation (this simplification is not strictly necessary), cone angle α can be directly deduced from the optical properties of the sail introduced in Eq. (1). The relation is obtained by solving:

$$\tan\alpha = \max_{\beta\in[0,\frac{\pi}{2}]} \frac{\boldsymbol{f}_{SRP}\cdot\hat{\boldsymbol{s}}}{\left\|\left(\mathbb{I}-\hat{\boldsymbol{s}}\hat{\boldsymbol{s}}^T\right)\boldsymbol{f}_{SRP}\right\|} = \max_{\beta\in[0,\frac{\pi}{2}]} \frac{\rho\, s\sin 2\beta + B_f\rho(1-s)\sin\beta}{1+\rho\, s\cos 2\beta + B_f\rho(1-s)\cos\beta}. \tag{5}$$

This condition holds for:

$$\beta^* = \cos^{-1}\left(\frac{-B_f\rho(1-s)(3\rho s+1)+\sqrt{B_f^2\rho^2(1-s)^2((3\rho s-1)^2-4\rho s)-32\rho^2 s^2(\rho s-1)}}{8\rho s}\right).$$

If $B_f = 0$, Eq. (5) simplifies to

$$\alpha(\rho,s) = \tan^{-1}\left(\frac{\rho\, s}{\sqrt{1-\rho^2\, s^2}}\right), \qquad \rho\, s = \frac{\tan\alpha}{\sqrt{1+\tan^2\alpha}}. \tag{6}$$

Hence, Eq. (4) is finally recast into

$$\begin{aligned} &\text{if } \exists\ p_I\in T^*M,\ p_I\neq 0 \text{ such that} \\ &\qquad \left\langle p_I,\ \tilde{G}(I,f)\,\boldsymbol{u}\right\rangle > 0, \qquad f\in\mathbb{S}^1,\ \boldsymbol{u}\in K_\alpha. \end{aligned} \tag{7}$$

A. Constructive approach to verify the controllability condition

A practical check of the feasibility Problem (7) is carried out by solving the auxiliary optimization problem

$$\begin{aligned} &\max_{J,\ \|p_I\|\leq 1} J \quad \text{s.t.} \\ &\qquad \left\langle p_I,\ \tilde{G}(I,f)\,\boldsymbol{u}\right\rangle \geq J,\ f\in\mathbb{S}^1,\ \boldsymbol{u}\in\partial K_\alpha,\ \|\boldsymbol{u}\|=1. \end{aligned} \tag{8}$$

The constraint $\|p_I\|\leq 1$ is preferred to $\|p_I\|=1$ to preserve convexity of Problem (8). Problem (8) is convex and semi-infinite, because inequality constraints need to be enforced on two

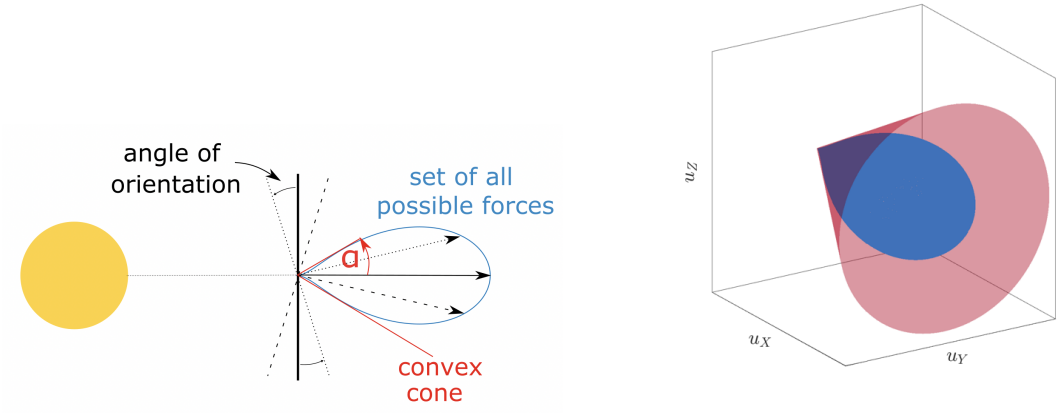

(a) Schematic representation

(b) Three-dimensional representation

Fig. 4: Approximation of the control set (blue) by a convex cone (red).

infinite sets, namely for all true anomalies between 0 and 2π and for all $\boldsymbol{u}$ on the surface of the cone. Evaluating inequalities in the interior of the cone is not necessary because dynamics is affine in $\boldsymbol{u}$. If J^*, solution of Problem (8), is positive, (7) is verified: then, as discussed in the previous section, for the cone angle α, there is an obstruction to local controllability around the orbit I. Conversely, when (3) holds at I[7], both J^* and the associated minimizer p_I must be zero.

To emphasize the practical interest of Problem (8), Figure 5 depicts an example solution for a given orbit as a function of α (the detailed numerical algorithm to achieve these solutions is provided in Section IV B). One can check that a minimum cone angle exists (for the specific I used in this simulation) for which (7) (and the corresponding obstruction to local controllability) cannot hold. This angle can be mapped into minimal requirements for the reflectivity of the sail

[7] In practice, of course, the check can only be made at a single point, while the condition must hold for all I to ensure global controllability.

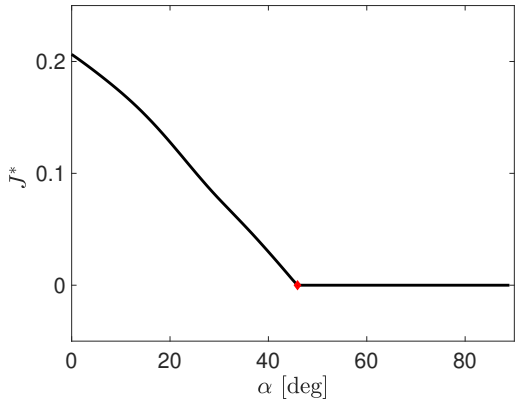

Fig. 5: Example of the solution of Problems (8) (black curve) and (9) (red dot). Here, $\gamma_2 = 50\,\text{deg}$, $\gamma_3 = 40\,\text{deg}$, and $e = 0.7$.

via Eq. (6), and it can be evaluated by solving

$$\begin{aligned} \min_{\alpha} \ \ & \alpha \qquad \text{s.t.} \\ & J^*(\alpha) = 0 \end{aligned} \tag{9}$$

where $J^*(\alpha)$ denotes solution of Problem (8) for a given α.

B. Optimization problem

Numerical solution of Problem (8) is achieved by using the formalism of positive trigonometric polynomials [12, 13] to enforce positivity constraints for all values of f and $\boldsymbol{u}$ without introducing any relaxation or discretization of the problem.

Let δ be an angle parametrizing control vectors on the surface of the cone, as shown in Fig. 6,

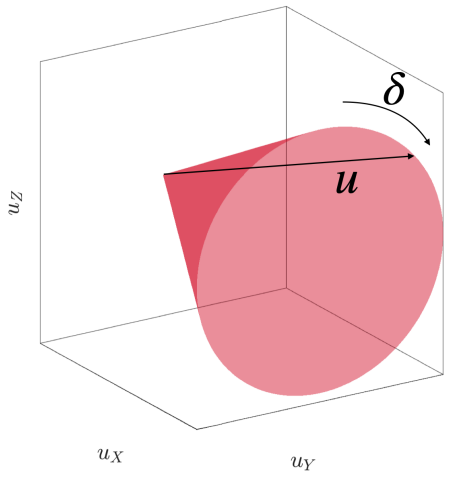

Fig. 6: Parametrization of the control vector.

namely

$$\boldsymbol{u} = \begin{bmatrix} \cos\alpha \\ \cos\delta \ \sin\alpha \\ \sin\delta \ \sin\alpha \end{bmatrix}$$

Positivity of the following constraints must be verified:

$$p_I^T \tilde{G}(I,f)\boldsymbol{u} - J \geq 0 \quad f \in \mathbb{S}^1, \quad \boldsymbol{u} \in \partial K_\alpha. \tag{10}$$

Inspection of $\tilde{G}(I,f)\boldsymbol{u}$ reveals that Eq. (10) is a bivariate trigonometric polynomial of second degree in f and first degree in δ. Let $\langle \cdot, \cdot \rangle_H$ be the Hermitian product of two complex-valued vectors, *i.e.*, $\langle a, b \rangle_H = \langle \mathrm{Re}(a), \mathrm{Re}(b) \rangle + \langle \mathrm{Im}(a), \mathrm{Im}(b) \rangle$, and denote $\Phi(f,\delta) = \left[1, \ \mathrm{e}^{i\delta}\right]^T \otimes \left[1, \ \mathrm{e}^{if}, \ \mathrm{e}^{2if}\right]^T = \left[1, \ \mathrm{e}^{if}, \ \mathrm{e}^{2if}, \ \mathrm{e}^{i\delta}, \ \mathrm{e}^{if}\mathrm{e}^{i\delta}, \ \mathrm{e}^{2if}\mathrm{e}^{i\delta}\right]^T$ the basis of bivariate trigonometric polynomials of degree 2 in f and 1 in δ, respectively (here, $\otimes$ denotes Kronecker's product). The left-hand term of Eq.(10)

can be reformulated as

$$\left\langle p_I,\ \tilde{G}(I,f)\,\boldsymbol{u}\right\rangle - J = p_I^T\left(\sum_{l=-1}^{1}\sum_{k=-2}^{2}\widetilde{Gu}^{(k,l)}\mathrm{e}^{i\,k\,f}\,\mathrm{e}^{i\,l\,\delta}\right) - J = \left\langle \Phi(f,\delta),\ \widetilde{Gu}\,p_I - \boldsymbol{e_1}J\right\rangle_H$$

where $\widetilde{Gu}^{(k,l)}(I)$ is the kl-th coefficient of the Fourier transform[8] of $\tilde{G}(I,f)\boldsymbol{u}$, and $\boldsymbol{e_1} = [1,0,0,0,0,0]^T$.

The formalism of squared functional systems outlined in [12] and [13] allows to recast the continuous positivity constraints into LMI. The corresponding squared functional system of $\Phi(f,\delta)$ is $\mathcal{S}^2(f,\delta) = \Phi(f,\delta)\Phi^H(f,\delta)$, where $\Phi^H(f,\delta)$ denotes conjugate transpose of $\Phi(f,\delta)$. Let N be the dimension of $\Phi(f,\delta)$ (6 in our application) and $\Lambda_H : \mathbb{C}^N \to \mathbb{C}^{N\times N}$ be a linear operator mapping coefficients of polynomials in $\Phi(f,\delta)$ to the squared base, so that application of Λ_H on $\Phi(f,\delta)$ yields

$$\Lambda_H(\Phi(f,\delta)) = \Phi(f,\delta)\Phi^H(f,\delta)$$

and define its adjoint operator $\Lambda_H^* : \mathbb{C}^{N\times N} \to \mathbb{C}^N$ as

$$\left\langle Y,\ \Lambda_H(\widetilde{Gu})\right\rangle_H \equiv \left\langle \Lambda_H^*(Y),\ \widetilde{Gu}\right\rangle_H, \quad Y \in \mathbb{C}^{N\times N}, \quad \widetilde{Gu} \in \mathbb{C}^N.$$

Theory of squared functional systems postulated by Nesterov [12] proves that trigonometric polynomial is non-negative if and only if a Hermitian positive semidefinite matrix Y exists such that $\widetilde{Gu} = \Lambda_H^*(Y)$. Dumitrescu extends this theory for multivariate trigonometric polynomials in [13, Chap. 3] and shows that all nonnegative bivariate trigonometric polynomials can be written as sum-of-squares. This equivalence is false for three or more variables.

Thus, $\left\langle \Phi(f,\delta), \widetilde{Gu}\right\rangle_H$ is non-negative for all $f \in \mathbb{S}^1$ and for all $\boldsymbol{u} \in K_\alpha$ if and only if a Hermitian positive semidefinite matrix Y exists such that $\widetilde{Gu} = \Lambda_H^*(Y)$, namely

$$\left\langle \Phi(f,\delta),\ \widetilde{Gu}\right\rangle_H \geq 0,\ f \in \mathbb{S}^1,\ \boldsymbol{u} \in K_\alpha \quad \Longleftrightarrow \quad \exists Y \succeq 0 :\ \widetilde{Gu} = \Lambda_H^*(Y).$$

[8] We note that $\tilde{G}^{kl} = \overline{\tilde{G}^{(-k,--l)}}$ because $\tilde{G}(I,f)\boldsymbol{u}$ is real valued.

In fact, it holds in this case that

$$\begin{aligned}\left\langle \Phi(f,\delta),\ c\right\rangle_H &= \left\langle \Phi(f,\delta),\ \Lambda_H^*(Y)\right\rangle_H = \left\langle \Lambda_H(\Phi(f,\delta)),\ Y\right\rangle_H,\\ &= \left\langle \Phi(f,\delta)\Phi^H(f,\delta),\ Y\right\rangle_H = \Phi^H(f,\delta)\, Y\, \Phi(f,\delta) \geq 0.\end{aligned}$$

For trigonometric polynomials Λ^* is given by

$$\Lambda_H^*(Y) = \begin{bmatrix} \mathrm{tr}(\langle Y,\ T_{00}\rangle) \\ \vdots \\ \mathrm{tr}(\langle Y,\ T_{kl}\rangle) \\ \vdots \\ \mathrm{tr}(\langle Y,\ T_{21}\rangle) \end{bmatrix} \quad k = 0,1,2,\ l = 0,1.$$

where T_j $j = 0,1,2$ are the elementary Toeplitz matrices with ones on the j-th diagonal and zeros elsewhere and T_{kl} are obtained from a Kronecker product of such matrices, *e.g.*,

$$T_0 = \begin{pmatrix} 1 & 0 \\ 0 & 1 \end{pmatrix}, \quad T_1 = \begin{pmatrix} 0 & 1 & 0 \\ 0 & 0 & 1 \\ 0 & 0 & 0 \end{pmatrix}, \quad T_{10} = T_0 \otimes T_1 = \begin{pmatrix} 0 & 1 & 0 & 0 & 0 & 0 \\ 0 & 0 & 1 & 0 & 0 & 0 \\ 0 & 0 & 0 & 0 & 0 & 0 \\ 0 & 0 & 0 & 0 & 1 & 0 \\ 0 & 0 & 0 & 0 & 0 & 1 \\ 0 & 0 & 0 & 0 & 0 & 0 \end{pmatrix}$$

Finally, the inequality in Eq. (10) is rewritten as an LMI:

$$\left\langle p_I,\ \tilde{G}(I,f)\,\boldsymbol{u}\right\rangle - J \geq 0,\ f \in \mathbb{S}^1,\ \boldsymbol{u} \in \partial K_\alpha \quad \Longleftrightarrow \quad \exists\, Y \succeq 0 \ \text{ such that } \ \widetilde{Gu}\, p_I - \boldsymbol{e_1} J = \Lambda_H^*(Y)$$

where $Y \in \mathbb{C}^{6\times 6}$ is a Hermitian matrix to be determined. Hence, the finite-dimensional counterpart

of Problem (8) is

$$\begin{aligned} \min_{J,\,\|p_I\|\leq 1,\,Y\in\mathbb{C}^{6\times 6}} \quad & J \quad \text{s.t.:} \\ & Y \succeq 0 \\ & \Lambda_H^*(Y) = \widetilde{Gu}\, p_I - \boldsymbol{e_1} J \end{aligned} \tag{11}$$

Eventually, solution of Problem (9) is carried out by means of a simple bisection algorithm. The CVX software [22, 23] is used to solve the convex Problem (11). Fourier coefficients of $\tilde{G}(I, f)$ are evaluated by means of the fast Fourier transform (FFT) algorithm.

We stress that there is no relaxation of Problem (11) with respect to Problem (8). Remarkably, enforcement of the constraint for all values of f and $\boldsymbol{u}$ is exact and stems from the trigonometric nature of $\tilde{G}(I, f)\boldsymbol{u}$. Hence, this methodology outperforms the algorithm that we proposed in [20], where controls necessary to move towards the vertexes of a simplex encompassing I where explicitly evaluated. In that case, a large number of harmonics was necessary to model the control variable and, eventually, to achieve a conservative estimate of the minimal cone angle α, as depicted in Fig. 7.

V. Minimal optical requirements

Figure 8 shows the minimum cone angle satisfying the condition as a function of γ_2 and γ_3 for various values of eccentricity (we recall that semi-major axis and γ_1 have no influence on this angle). The minimal angle is symmetric with respect to $\gamma_2 = 90\,\text{deg}$ because $\left\langle p_I,\ \tilde{G}(e, \gamma_2, \gamma_3, f)\,\boldsymbol{u} \right\rangle = \left\langle -p_I,\ \tilde{G}(e, \pi - \gamma_2, \gamma_3, f)\,\boldsymbol{u} \right\rangle$. Solution is independent of γ_3 for circular orbits, as expected. Sensitivity with respect to γ_3 remains moderate even for larger eccentricities. The minimal angle approaches zero as $\sin(\gamma_2) \to 0$. In this case, $\hat{\boldsymbol{s}}$ is aligned with the angular momentum of the orbit. On the other hand, for $\gamma_2 = 90\,\text{deg}$, the Sun is in the orbital plane.

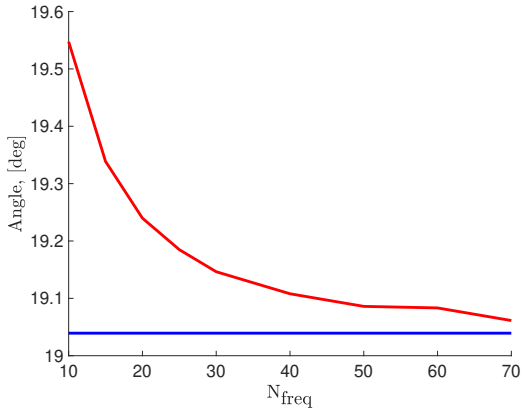

Fig. 7: Convergence of the results obtained in [20] as the number of harmonics increases (in red) towards the minimum angle obtained with the methodology detailed in this paper (in blue).

Figure 9 represents α_{min} as function of γ_3 or γ_2 (Fig. 9a and 9b, respectively) for various values of eccentricity. Results confirm high dependency of α_{min} on γ_2, and γ_3 for large eccentricity. Hence, controllability of near circular orbits requires more reflective sails with respect to high-eccentric orbits. Finally, we stress that the minimum angle α exists for all orbits, and it is systematically smaller than 90 deg, which means that the sail has not to be ideal to make System (2) controllable. To compare with a real solar sail, optical properties of the NASA reference model [24] (designed to support NEA Scout and Lunar Flashlight solar sail missions) correspond to a cone angle of 58.6 deg. This value is sufficient to satisfy the proposed condition for most planet-centered orbits, except for highly inclined ones.

A. A comment on heliocentric orbits

Consider now a sail in a heliocentric orbit. This scenario can be a case for interplanetary transfers, for example. The same equations with two major corrections are used to model the problem.

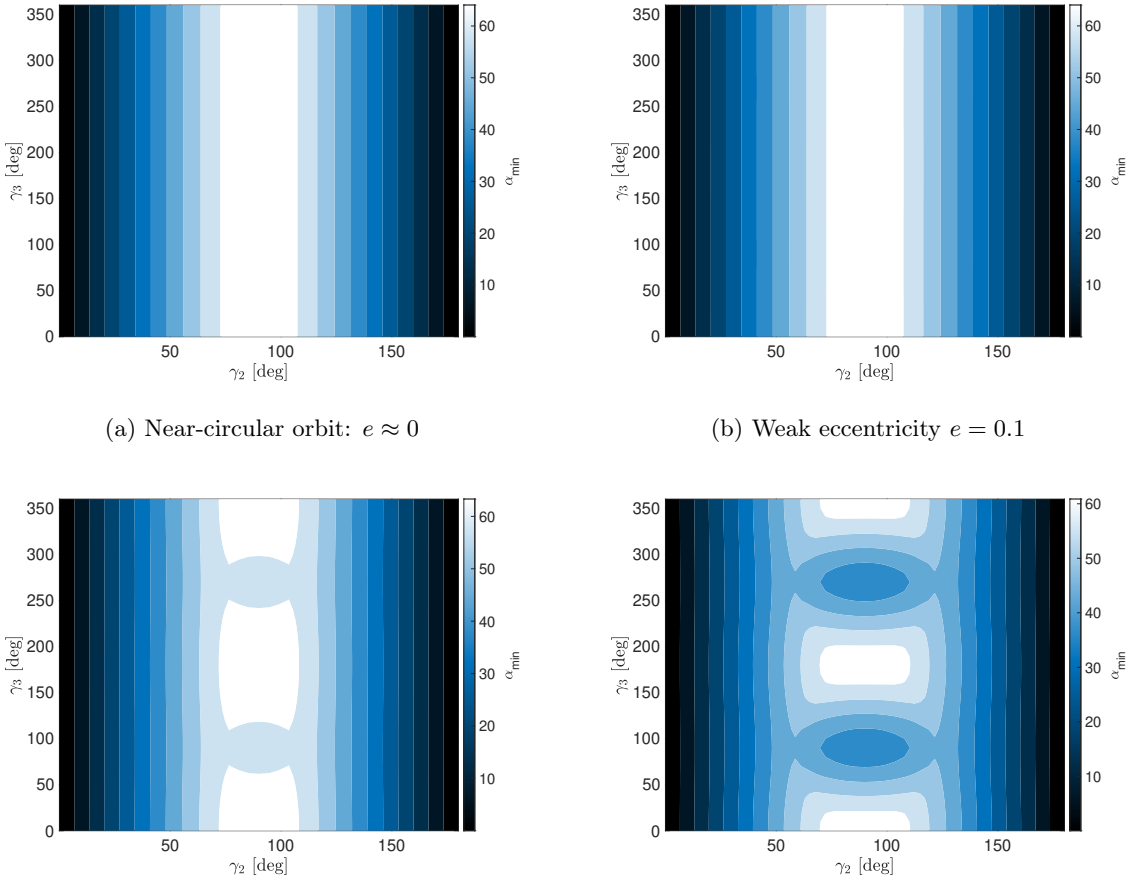

(a) Near-circular orbit: $e \approx 0$

(b) Weak eccentricity $e = 0.1$

(c) Elliptic orbit with $e = 0.5$

(d) High eccentricity $e = 0.9$

Fig. 8: Results for different geocentric orbits

First, the rotation matrix R in Eq. (2) is removed, since the local vertical local horizontal frame is used, and $\hat{\boldsymbol{s}}$ is aligned with the radial direction. Moreover, the problem has central symmetry, so that results do not depend on any orbital element except for the eccentricity. For a perfectly absorptive solar sail, the dynamical system is not bracket generating, because the control is radial, as proved in [25]. The integral of motion related to this rank deficiency is the magnitude of the angular momentum. For a non-ideal sail, the system becomes bracket generating as soon as a

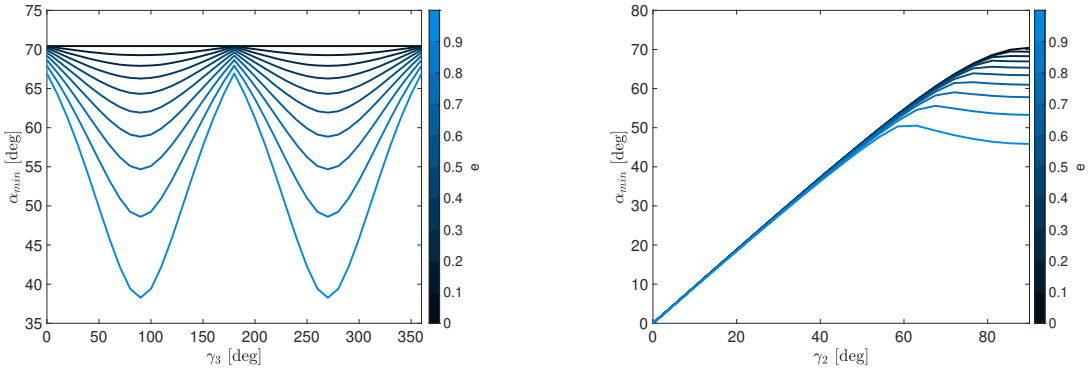

(a) γ_2 fixed at 90 [deg]

(b) γ_3 fixed at 120 [deg]

Fig. 9: Minimum cone angle as a function of Euler angles.

tangential component appears: even for very weakly reflective sails.

Using the methodology of Section IV indicates that even a very poorly reflective sail (*i. e.*, $0 < \rho \ll 1$) is locally controllable over an orbital period. However, an orbital period of heliocentric orbits is of the order of the year, this is why the proposed methodology is not well suitable to tackle realistic mission scenario of interplanetary transfers using solar sails. In fact, a sail can be moved towards any direction of the tangent manifold of the orbital elements set, but the requirement is unaware of the orbital period's magnitude, so that these maneuvers could possibly last for years.

VI. Conclusion

We introduced a novel requirement to assess the controllability of solar sails in orbit around a celestial body. This was formulated as a geometric condition on the reachable set of orbits (slow variables of the system, in contrast with longitude which is the fast one). A failure of this requirement typically indicates that a half neighborhood of the state vector exists where the sail cannot be moved. A numerical algorithm based on convex optimization and leveraging on the theory

of square functional systems for trigonometric polynomials was proposed to efficiently evaluate this requirement. Extensive exploitation of the algorithm revealed that any orbital condition can tolerate a certain amount of absorption of solar radiation. A remarkable byproduct of this analysis is that local controllability properties hold universally (that is for all orbital conditions) for non-ideal sails provided a sufficient amount of incoming radiation is reflected.

VII. Acknowledgements

This work was partially supported by ESA (contract no. 4000134950/21/NL/GLC/my).

APPENDIX A: LIE BRACKETS COMPUTATION FOR A PERFECTLY-ABSORPTIVE SAIL

Consider a control-affine dynamical system

$$\dot{x} = F^0(x) + \sum_{i=1}^{m} u_i F^i(x), \quad x \in \mathcal{M}, \quad \boldsymbol{u} = (u_1, \ldots, u_m) \in U \subset \mathbb{R}^m \tag{A1}$$

where $\mathcal{M}$ is an n-dimensional manifold, $F^i : \mathcal{M} \to T\mathcal{M}$ are smooth vector fields on $\mathcal{M}$. We note that Eq. (2) can be recast into the form of Eq. (A1) by choosing columns of $G(I, f)R(I, f)$ as vector fields F^i.

To compute Lie algebra, only directions of vector fields matter. To simplify, assume that control system is given by a simple two-body equation with a term of perturbation, as denoted in (A2) with $\hat{\boldsymbol{s}}$ solar vector, considered fixed for a few orbits. For a perfectly absorptive solar sail, only the cross-sectional surface is controlled, so that control is assumed to be $u \in [0, 1]$ with a certain coefficient ε defining SRP magnitude.

Using $x = (\boldsymbol{r}, \boldsymbol{v}) \in \mathbb{R}^6$ as state vector, where $\boldsymbol{r}$ and $\boldsymbol{v}$ denote Cartesian position and velocity

vectors, respectively, System (A2) can be rewritten as:

$$\dot{x} = F^0(x) + \varepsilon\, u F^1(x)$$

with F^0 the recurrent drift and F^1 the SRP perturbation.

$$\begin{cases} \dfrac{\mathrm{d}\,\boldsymbol{r}}{\mathrm{d}\,t} = \boldsymbol{v} \\ \\ \dfrac{\mathrm{d}\,\boldsymbol{v}}{\mathrm{d}\,t} = -\dfrac{\mu}{r^3}\boldsymbol{r} + \varepsilon(r_\odot)\,\hat{\boldsymbol{s}} u \end{cases} \tag{A2}$$

where $r = \|\boldsymbol{r}\|$. System (A2) provides two vector fields:

$$\begin{aligned} F^0 &= v_X \frac{\partial}{\partial r_X} + v_Y \frac{\partial}{\partial r_Y} + v_Z \frac{\partial}{\partial r_Z} - \frac{r_X}{r^3}\frac{\partial}{\partial v_X} - \frac{r_Y}{r^3}\frac{\partial}{\partial v_Y} - \frac{r_Z}{r^3}\frac{\partial}{\partial v_Z} \\ F^1 &= s_X \frac{\partial}{\partial v_X} + s_Y \frac{\partial}{\partial v_Y} + s_Z \frac{\partial}{\partial v_Z} \end{aligned}$$

To simplify, let us denote vector fields:

$$\begin{aligned} v\frac{\partial}{\partial r} &= v_X \frac{\partial}{\partial r_X} + v_Y \frac{\partial}{\partial r_Y} + v_Z \frac{\partial}{\partial r_Z}, \quad \frac{r}{r^3}\frac{\partial}{\partial v} = \frac{r_X}{r^3}\frac{\partial}{\partial v_X} + \frac{r_Y}{r^3}\frac{\partial}{\partial v_Y} + \frac{r_Z}{r^3}\frac{\partial}{\partial v_Z} \\ s\frac{\partial}{\partial v} &= s_X \frac{\partial}{\partial v_X} + s_Y \frac{\partial}{\partial v_Y} + s_Z \frac{\partial}{\partial v_Z} \end{aligned}$$

and

$$F^{sr} = s\frac{\partial}{\partial r},\ F^{rr} = r\frac{\partial}{\partial r},\ F^{vr} = v\frac{\partial}{\partial r},\ F^{sv} = s\frac{\partial}{\partial v},\ \ldots$$

Finally, by denoting $\hat{\boldsymbol{s}} \cdot \boldsymbol{r}$ a scalar product of two vectors $\hat{\boldsymbol{s}}$ and $\boldsymbol{r}$, computation of Lie brackets gives

the following results:

$$F^0 = v\frac{\partial}{\partial r} - \frac{r}{r^3}\frac{\partial}{\partial v} = F^{vr} - \frac{1}{r^3}F^{rv}; \quad F^1 = s\frac{\partial}{\partial v} = F^{sv}; \quad F^{01} = \Big[F^0, F^1\Big] = -F^{sr}$$

$$F^{001} = \Big[F^0, [F^0, F^1]\Big] = \frac{3\,(\hat{\boldsymbol{s}}\cdot\boldsymbol{r})}{r^5}\,F^{rv} - \frac{F^{sv}}{r^3}, \quad F^{101} = \Big[F^1, [F^0, F^1]\Big] = 0$$

$$F^{0001} = \Big[F^0, [F^0, [F^0, F^1]]\Big] = \frac{1}{r^3}F^{sr} + \frac{3(\boldsymbol{v}\cdot\boldsymbol{r})}{r^5}F^{sv} + \Big(\frac{3(\hat{\boldsymbol{s}}\cdot\boldsymbol{v})}{r^5} - \frac{15(\hat{\boldsymbol{s}}\cdot\boldsymbol{r})(\boldsymbol{v}\cdot\boldsymbol{r})}{r^7}\Big)F^{rv}$$
$$+ \frac{3(\hat{\boldsymbol{s}}\cdot\boldsymbol{r})}{r^5}(F^{vv} - F^{rr})$$

All subsequent iterations are linear combinations of the previous vector fields. Thus, Lie algebra of the system (A2) has 5 independent vector fields if $\hat{\boldsymbol{s}}\cdot\boldsymbol{r} \neq 0$:

$$F^{sr},\ F^{sv},\ F^{rv},\ F^{vr},\ F^{vv} - F^{rr}\,.$$

$$\dim \mathrm{Lie}(F^0, F^1, ...) = 5 \quad < \quad \dim \mathbb{R}^6 = 6$$

Moreover, rank deficiency implies that an integral of motion exists, which happens to be the projection of the angular momentum $\boldsymbol{h}$ towards $\hat{\boldsymbol{s}}$, namely $\hat{\boldsymbol{s}}\cdot\boldsymbol{h} = \hat{\boldsymbol{s}}\cdot(\boldsymbol{r}\times\boldsymbol{v}) = \det(\boldsymbol{r},\boldsymbol{v},\hat{\boldsymbol{s}})$ In fact, Lie derivative of $\hat{\boldsymbol{s}}\cdot\boldsymbol{h}$ with respect to the controlled vector field, $F^1 = s_X\frac{\partial}{\partial v_X} + s_Y\frac{\partial}{\partial v_Y} + s_Z\frac{\partial}{\partial v_Z}$ is:

$$\begin{aligned} L_{F^1}(\det(\boldsymbol{r},\boldsymbol{v},\hat{\boldsymbol{s}})) &= s_X\frac{\partial}{\partial v_X}\det(\boldsymbol{r},\boldsymbol{v},\hat{\boldsymbol{s}}) + s_Y\frac{\partial}{\partial v_Y}\det(\boldsymbol{r},\boldsymbol{v},\hat{\boldsymbol{s}}) + s_Z\frac{\partial}{\partial v_Z}\det(\boldsymbol{r},\boldsymbol{v},\hat{\boldsymbol{s}}) \\ &= s_X(-r_Y s_Z + r_Z s_Y) + s_Y(r_X s_Z - r_Z s_X) + s_Z(-r_X s_Y + r_Y s_X) \\ &= 0 \end{aligned}$$

REFERENCES

[1] McInnes, C. R., *Solar Sailing*, Springer London, 1999. doi:10.1007/978-1-4471-3992-8.

[2] Macdonald, M., McInnes, C., and Dachwald, B., "Heliocentric Solar Sail Orbit Transfers with Locally Optimal Control Laws," *Journal of Spacecraft and Rockets*, Vol. 44, 01 2007, pp. 273–276. doi: 10.2514/1.17297.

[3] Gong, S. p., Gao, Y.-F., and Li, J., "Solar sail time-optimal interplanetary transfer trajectory design," *Research in Astronomy and Astrophysics*, Vol. 11, 07 2011, pp. 981. doi:10.1088/1674-4527/11/8/010.

[4] Dachwald, B., "Optimal Solar Sail Trajectories for Missions to the Outer Solar System," *AIAA/AAS Astrodynamics Specialist Conference and Exhibit*, American Institute of Aeronautics and Astronautics, jun 2004. doi:10.2514/6.2004-5406.

[5] Mengali, G. and Quarta, A., "Near-Optimal Solar-Sail Orbit-Raising from Low Earth Orbit," *Journal of Spacecraft and Rockets*, Vol. 42, 09 2005, pp. 954–958. doi:10.2514/1.14184.

[6] Colombo, C., Miguel Banos, N., and Gkolias, I., "Modulating Solar Sail Control for End-Of-life Disposal with Solar Sails," *5th International Symposium on Solar Sailing*, Aachen, Germany, 2019.

[7] Niccolai, L., Quarta, A., and Mengali, G., "Solar sail heliocentric transfers with a Q-law," *Acta Astronautica*, Vol. 188, 11 2021, pp. 352–361. doi:10.1016/j.actaastro.2021.07.037.

[8] Caruso, A., Bassetto, M., Mengali, G., and Quarta, A. A., "Optimal solar sail trajectory approximation with finite Fourier series," *Advances in Space Research*, Vol. 67, No. 9, 2021, pp. 2834–2843. doi: https://doi.org/10.1016/j.asr.2019.11.019, Solar Sailing: Concepts, Technology, and Missions II.

[9] Kim, M. and Hall, C., "Symmetries in the Optimal Control of Solar Sail Spacecraft," *Celestial Mechanics and Dynamical Astronomy*, Vol. 92, 08 2005, pp. 273–293. doi:10.1007/s10569-004-2530-x.

[10] Sullo, N., Peloni, A., and Ceriotti, M., "Low-Thrust to Solar-Sail Trajectories: A Homotopic Approach," *Journal of Guidance, Control, and Dynamics*, Vol. 40, No. 11, nov 2017, pp. 2796–2806. doi:10.2514/1.g002552.

[11] Pellegrino, M. and Scheeres, D. J., "Reachability of a Passive Solar Sail in Earth Orbit," *Journal of Guidance, Control, and Dynamics*, Vol. 44, No. 2, feb 2021, pp. 360–369. doi:10.2514/1.g005264.

[12] Nesterov, Y., "Squared Functional Systems and Optimization Problems," *High Performance Optimization*, edited by P. M. Pardalos, D. Hearn, H. Frenk, K. Roos, T. Terlaky, and S. Zhang, Vol. 33, Springer US, Boston, MA, 2000, pp. 405–440. doi:10.1007/978-1-4757-3216-0_17, Series Title: Applied Optimization.

[13] Dumitrescu, B., *Positive Trigonometric Polynomials and Signal Processing Applications*, Springer Netherlands, 2007. doi:10.1007/978-1-4020-5125-8.

[14] Dachwald, B., Macdonald, M., McInnes, C. R., Mengali, G., and Quarta, A. A., "Impact of Optical Degradation on Solar Sail Mission Performance," *Journal of Spacecraft and Rockets*, Vol. 44, No. 4, July 2007, pp. 740–749. doi:10.2514/1.21432.

[15] Montenbruck, O. and Gill, E., *Satellite Orbits*, Springer Science + Business Media, 2000. doi: 10.1007/978-3-642-58351-3.

[16] Rios-Reyes, L. and Scheeres, D. J., "Generalized Model for Solar Sails," *Journal of Spacecraft and Rockets*, Vol. 42, No. 1, jan 2005, pp. 182–185. doi:10.2514/1.9054.

[17] Bonnard, B., "Contrôlabilité des systèmes non linéaires," *C. R. Acad. Sci. Paris Sér. I Math.*, Vol. 292, No. 10, 1981, pp. 535–537.

[18] Jurdjevic, V., *Geometric Control Theory*, Cambridge University Press, 1st ed., 1996. doi: 10.1017/CBO9780511530036.

[19] Scheeres, D. J., *Orbital Motion in Strongly Perturbed Environments*, Springer Berlin Heidelberg, 2012. doi:10.1007/978-3-642-03256-1.

[20] Herasimenka, A., Caillau, J., Dell'Elce, L., and Pomet, J., "Controllability Test for Fast-Oscillating Systems with Constrained Control. Application to Solar Sailing," *2022 European Control Conference (ECC)*, 2022, pp. 2143–2148. doi:10.23919/ECC55457.2022.9838146.

[21] Caillau, J.-B., Dell'Elce, L., Herasimenka, A., and Pomet, J.-B., "On the Controllability of Nonlinear Systems with a Periodic Drift," 2022, HAL preprint no. 03779482.

[22] Grant, M. and Boyd, S., "CVX: Matlab Software for Disciplined Convex Programming, version 2.1," `http://cvxr.com/cvx`, March 2014.

[23] Grant, M. and Boyd, S., "Graph implementations for nonsmooth convex programs," *Recent Advances in Learning and Control*, edited by V. Blondel, S. Boyd, and H. Kimura, Lecture Notes in Control and Information Sciences, Springer-Verlag Limited, 2008, pp. 95–110, `http://stanford.edu/~boyd/graph_dcp.html`.

[24] Heaton, A. F. and Artusio-Glimpse, A., "An Update to the NASA Reference Solar Sail Thrust Model," *AIAA SPACE 2015 Conference and Exposition*, American Institute of Aeronautics and Astronautics, aug 2015. doi:10.2514/6.2015-4506.

[25] Bonnard, B., Caillau, J.-B., and Trélat, E., "Geometric optimal control of elliptic Keplerian orbits," *Discrete & Continuous Dynamical Systems - B*, Vol. 5, No. 4, 2005, pp. 929–956. doi: 10.3934/dcdsb.2005.5.929.